

1 Removing the North Pacific halocline: effects on global
2 climate, ocean circulation and the carbon cycle

3 L.Menviel^a, A. Timmermann^b, O. Elison Timm^b, A. Mouchet^c, A.
4 Abe-Ouchi^{e,d}, M.O. Chikamoto^e, N. Harada^e, R. Ohgaito^e, Y. Okazaki^e

5 ^a*Climate and Environmental Physics, Oeschger Centre for Climate Change Research,*
6 *University of Bern, Sidlerstrasse 5, CH-3012 Bern, Switzerland*

7 ^b*IPRC, SOEST, University of Hawai'i, 2525 Correa Road, Honolulu, HI 96822, USA*

8 ^c*Département AGO, Université de Liège, Liège, Belgium*

9 ^d*Atmosphere Ocean Research Institute, University of Tokyo, Japan*

10 ^e*Research Institute for Global Change, Japan Agency for Marine Science and*
11 *Technology, Japan*

12 **Abstract**

13 A well pronounced halocline is a key feature of today's subarctic North Pa-
14 cific. There is indirect paleo-evidence from the last glacial termination as well
15 as from the early and middle Pliocene that this halocline has not always been
16 there. To study the effects North Pacific salinity on global climate, ocean
17 circulation and the marine carbon-cycle, we perform idealized experiments
18 using an Earth system model of intermediate complexity (LOVECLIM). Im-
19 posing a negative freshwater flux in the northern North Pacific, the halocline
20 vanishes and a deep Pacific Meridional Overturning Circulation (PMOC) es-
21 tablishes. The associated increase of meridional heat transport in the Pacific
22 leads to a bipolar seesaw response in temperature, with warming in the North
23 Pacific and over North America and cooling in the Southern Ocean. As a
24 result of the formation of North Pacific Deep Water (NPDW), the surface
25 branch of the global conveyor belt circulation weakens. Transport through
26 the Indonesian Seas decreases by 50% as the warm and saline water of the

*Corresponding author
Preprint submitted to Deep Sea Research
Email address: menviel@climate.unibe.ch (L.Menviel)

October 5, 2010

27 equatorial Pacific are diverted into the North Pacific.

In our idealized experiments, the enhanced global deep water formation is balanced by an increase in diapycnal mixing. As a result nutrient concentrations in the euphotic zone increase by about 25% globally, leading to a 20% increase in global export production. The effect of greater export production on atmospheric $p\text{CO}_2$ is however compensated by an enhanced transport of Dissolved Inorganic Carbon (DIC) to the surface. As a result, the atmospheric CO_2 concentration increases by only 5 ppmv. Our results further suggest that the absence of the subarctic halocline for instance during Heinrich event 1 and the Pliocene may have exerted a strong influence on global climate and the carbon cycle.

28 *Keywords:* Pacific Meridional Overturning Circulation, carbon cycle,
29 Earth system model of Intermediate complexity, Climate change

30 **1. Introduction**

31 Under present-day conditions, deep water is formed in the North Atlantic
32 and not in the North Pacific. In the North Pacific surface salinity is relatively
33 low (~ 32.8 psu) compared to that of the underlying deep water (~ 34.6
34 psu) (Warren, 1983), thereby preventing the formation of Deep Waters. The
35 presence of a well-pronounced subarctic North Pacific Halocline (NPH) is
36 controlled by a number of different processes (see Emile-Geay et al. (2003)
37 and Kiefer (2010) for an overview):

- 38 • the atmospheric export of moisture from the Atlantic to the Pacific by
39 trade winds crossing Central America,
- 40 • a limited meridional cross-gyre flow of salty subtropical waters

- 41 • the positive freshwater balance associated with the East Asian Summer
42 Monsoon.

43 One key question to address is what long-term processes control the strength
44 of the NPH. During the early to middle Pliocene for example, when the
45 Panama Seaway was still open and allowed for the exchange of surface waters
46 and thermocline waters between the Atlantic and the Pacific, paleo-data
47 reveal a strong level of surface productivity in the subarctic North Pacific
48 which has been interpreted (Haug et al., 1999) in terms of the absence of a
49 NPH. This result was corroborated by a modeling study (Motoi et al., 2005)
50 in which an open Panama Isthmus caused an increase of surface salinity in
51 the North Pacific and even led to the formation of a Deep Pacific Meridional
52 Overturning cell. Motoi et al. (2005) furthermore argued that this may have
53 further delayed the build-up of Northern Hemispheric ice-sheets during the
54 Pliocene. Similar conclusions were drawn by (Haug et al., 2005).

55 Paleo-data as well as recent modeling experiments (Okazaki et al., 2010)
56 document that also during the last glacial termination the NPH may have
57 disappeared twice – during Heinrich event 1 and the Younger Dryas Period.
58 While during these periods the Atlantic Meridional Overturning Circulation
59 (AMOC) was substantially weaker than at present (McManus et al., 2004),
60 there is indirect paleo evidence for enhanced deep water ventilation in the
61 North Pacific (Ahagon et al., 2003; Ohkushi et al., 2004; Sagawa and Ikehara,
62 2008; Okazaki et al., 2010) that may have been caused by increased surface
63 salinities in the Bering Sea and the Gulf of Alaska. This scenario is also
64 consistent with previous modeling studies (Mikolajewicz et al., 1997; Saenko
65 et al., 2004; Krebs and Timmermann, 2007; Okazaki et al., 2010). The de-

66 velopment of a deep Pacific Meridional Overturning Circulation (PMOC) in
67 these model solutions increases the poleward heat transport in the North Pa-
68 cific, which leads to a warming of subpolar areas and parts of North America.

69 Influences of such dramatic reorganizations of the global conveyor belt cir-
70 culation on the carbon cycle and resulting potential feedbacks between North
71 Pacific climate and marine biogeochemical changes have, to our knowledge,
72 not been studied in great detail yet.

73 The objectives of this study are to study the impacts of removing the
74 NPH on ocean circulation, global climate and the carbon cycle. For that
75 purpose, we perform idealized experiments using an Earth system Model of
76 Intermediate Complexity (EMIC), LOVECLIM version 1.1. (Goosse et al.,
77 2010), in which we artificially impose negative freshwater fluxes in the north-
78 ern North Pacific. In section 2, we describe the experimental set-up of our
79 idealized modeling experiments in more detail. Section 3, discusses the cli-
80 mate and carbon cycle responses to the establishment of the PMOC. Finally
81 section 4 presents a summary and discussion of the main results.

82 **2. Model and experimental setup**

83 To study the impact of North Pacific salinity changes on the climate and
84 the carbon cycle system, we perform idealized sensitivity experiments using
85 the EMIC LOVECLIM, version 1.1. LOVECLIM is faster than GCMs be-
86 cause its atmospheric component is simplified and coarser than other GCMs.
87 As a result, longer experiments can be performed with a full coupling between
88 all the components of the climate and carbon cycle systems.

89 *2.1. The Earth-system model LOVECLIM*

90 The atmospheric component of the coupled model LOVECLIM is EC-
91 Bilt (Opsteegh et al., 1998), a spectral T21, three-level model, based on
92 quasi-geostrophic equations extended by estimates of ageostrophic terms
93 (Lim et al., 1991). The model contains a full hydrological cycle which is
94 closed over land by a bucket model for soil moisture and a runoff scheme.
95 Synoptic variability associated with weather patterns is explicitly computed.
96 Diabatic heating due to radiative fluxes, the release of latent heat and the
97 exchange of sensible heat with the surface are parametrized.

98 The sea ice-ocean component of LOVECLIM, CLIO (Goosse et al., 1999;
99 Goosse and Fichefet, 1999; Campin and Goosse, 1999) consists of a free-
100 surface primitive equation model with $3^\circ \times 3^\circ$ resolution coupled to a thermodynamic-
101 dynamic sea ice model. Coupling between atmosphere and ocean is done via
102 the exchange of freshwater and heat fluxes, rather than by virtual salt fluxes.
103 To avoid a singularity at the North Pole, the oceanic component makes use
104 of two subgrids: The first one is based on classic longitude and latitude coor-
105 dinates and covers the whole ocean except for the North Atlantic and Arctic
106 Ocean. These are covered by the second spherical subgrid, which is rotated
107 and has its poles at the equator in the Pacific (111°W) and Indian Ocean
108 (69°E).

109 The terrestrial vegetation module of LOVECLIM, VECODE (Brovkin
110 et al., 1997), computes once a year the evolution of the vegetation cover
111 based on annual mean values of several climatic variables. The vegetation
112 cover is described as a fractional distribution of desert, tree, and grass in
113 each land grid cell. Within the version of LOVECLIM used here, simulated

114 vegetation changes affect only the land-surface albedo, and have no influence
115 on other processes such as evapo-transpiration.

116 LOCH is a 3-dimensional global model of the oceanic carbon cycle sim-
117 ulating dissolved inorganic carbon (DIC), total alkalinity, ^{14}C , phosphates
118 (PO_4^{3-}), organic products, oxygen and silica (Mouchet and Francois, 1996;
119 Fichefet et al., 2007). LOCH is coupled to CLIO, with the same time step.
120 In addition to their biogeochemical transformations, tracers in LOCH expe-
121 rience the advection and diffusion predicted by CLIO. The uptake of CO_2
122 by the ocean is governed by the solubility as well as biological pumps. The
123 partial pressure of CO_2 in the surface waters is calculated from the total al-
124 kalinity and DIC tracers. The difference between the partial pressure of CO_2
125 in the ocean and in the atmosphere, modulated by an exchange coefficient
126 sets the CO_2 air-sea exchange rate. LOCH computes the export production
127 from the fate of a phytoplankton pool in the euphotic zone (0–120 m). The
128 phytoplankton growth depends on the availability of nutrients (PO_4^{3-}) and
129 light, with a weak temperature dependence. A grazing process together with
130 natural mortality limit the biomass of the primary producers and provide
131 the source term for the organic matter sinking to depth. Remineralization of
132 organic matter depends on oxygen availability, but anoxic remineralization
133 can also occur. Depending on the silica availability, phytoplankton growth
134 is accompanied by the formation of opal or CaCO_3 (calcite and aragonite)
135 shells, which then sink to depth. CaCO_3 shells are dissolved depending on
136 the calcite and aragonite saturation states, whereas a simple constant rate
137 is used for opal. The organic matter that is not remineralized and the shells
138 that are not dissolved are permanently preserved in the sediments. This leads

139 to a loss of alkalinity, carbon, phosphates and silica, which is compensated by
140 the river influx. The ^{14}C content at any point in the ocean is expressed as a
141 $^{14}\text{C}/^{12}\text{C}$ ratio. The production rate of ^{14}C is held constant. The atmospheric
142 CO_2 content is predicted for each ocean timestep from the air-sea CO_2 fluxes
143 calculated by LOCH as well as from the air-terrestrial biomass CO_2 fluxes
144 provided by VECODE.

145 *2.2. Experimental setup*

146 The pre-industrial steady state (**PIN**) was obtained by forcing LOVE-
147 CLIM with 278 ppmv of atmospheric CO_2 for 500 years, then allowing the
148 atmospheric CO_2 to vary freely for 700 years (Meniel et al., 2008). The
149 model is then forced with an atmospheric $\Delta^{14}\text{C}$ content of 0 permil for about
150 10,000 years, after which it is allowed to vary freely. All sensitivity experi-
151 ments start from this equilibrated simulation.

152 To remove the NPH and initiate the formation of North Pacific Deep
153 Water (NPDW) we extract freshwater in the area 150°E - 230°E , 47°N - 63°N
154 (Freshwater Experiment **FE**) under pre-industrial conditions and starting
155 from experiment **PIN**.. The overall duration of the applied forcing is 2,000
156 years. The magnitude of the negative freshwater forcing increases linearly
157 during the first 1,000 years to -0.3 Sv [$1\text{ Sv}=10^6\text{ m}^3/\text{s}$], a linear decrease at
158 a similar rate is applied for the following 1,000 years to return to the control
159 background conditions (figure 1). Experiment **FE** is highly idealized and the
160 negative freshwater forcing is chosen as a way to mimic paleo situations in
161 which the NPH was weak or absent, as was hypothesized for Heinrich event
162 1 or the early Pliocene. The length of the forcing (2,000 years) was chosen to
163 mimic the duration of Heinrich event 1, a time with probably higher salinities

164 in the subpolar North Pacific (Okazaki et al., 2010). The amplitude of the
165 forcing is set up such as to remove the halocline and generate a substantial
166 PMOC that extends into deep waters. In experiment **FE**, we close the Bering
167 Strait to prevent sea-level gradient-driven freshwater exchanges between the
168 Arctic Ocean and the North Pacific (Hu and Meehl, 2005). Experiment
169 **FE** was performed without global salinity compensation to avoid a biased
170 temperature response in the Southern Ocean (Stocker et al., 2007).

171 **3. Results**

172 *3.1. Oceanic response*

173 In response to the anomalous freshwater extraction in the northern North
174 Pacific, the sea surface salinity in the area 150°E-230°E, 50°N-60°N increases
175 by up to 2 after 1,000 years (figure 2) which is enough to remove the NPH.
176 This positive salinity anomaly causes an increase in surface water density
177 in the North Pacific by about 1.2 kg/m³. This positive density anomaly
178 leads to the gradual development of a deep overturning circulation in the
179 North Pacific (figure 1), as well as a slight weakening of the AMOC (figure
180 3, upper panels). After 1,000 years, the maximum overturning strength in
181 the Pacific (as measured by the maximum of the meridional streamfunction
182 in the North Pacific) attains values of up to 30 Sv and the newly formed
183 NPWD reaches a depth of 4000 m (figure 3, bottom right panel). A cross
184 equatorial transport of about 10 Sv establishes which leads to a reduction of
185 the volume of Antarctic Bottom Water (AABW) in the Pacific.

186 As illustrated by the winter mixed layer depth anomalies (figure 4, right
187 panel versus left panel) the major site of NPDW formation is the western part

188 of the Bering Sea, close to the coast of Kamchatka, but intensified mixing
189 also occurs elsewhere in the subarctic North Pacific. As a result of changes in
190 the overturning circulation the model simulates an increased poleward trans-
191 port of heat by 0.5 PW which is accompanied by a large-scale warming in the
192 North Pacific reaching maximum values of up to 7°C in the Sea of Okhotsk
193 and by 2.5°C, when averaged over 150°E-230°E, 50°N-60°N (figure 2). The
194 warmer conditions at the ocean surface can be related to a strong poleward
195 shift of the Kuroshio extension region (figure 4, right panel) creating condi-
196 tions that are somewhat analogous to the Gulf-Stream-North Atlantic Drift
197 configuration under present-day conditions. Moreover, the stronger merid-
198 ional component of the Kuroshio extending into supolar areas advects more
199 saline subtropical surface waters into the sinking regions, thereby providing a
200 positive feedback (Saenko et al., 2004; Okazaki et al., 2010). The upper ocean
201 (1000 m) poleward salinity transport at 35°N increases by ~200% compared
202 to **PIN**.

203 However, as soon as the imposed extraction of freshwater ceases (after
204 model year 2,000) NPDW formation stops. The inflow of warm water to the
205 North Pacific does not advect enough saline waters to maintain high surface
206 density. This suggests further that in our model solution the PMOC does
207 not exhibit any considerable hysteresis or saddle node bifurcation behaviour.
208 As can be seen in figure 5 (left panel), the NPDW that is being formed in the
209 Bering Sea is relatively warm whereas the southern hemisphere waters cool
210 down to 2000 m. Averaged over the entire Pacific, we observe a reduction
211 in intermediate to deep level stratification in the Pacific Ocean, in particular
212 between 40°S-10°N (figure 5, right panel). Since surface winds do not change

213 dramatically in experiment **FE** the globally increased formation of deep water
214 has to be balanced by enhanced diapycnal mixing. As will be shown below
215 this is essential for the global biogeochemical response in experiment **FE** .

216 Due to the formation of NPDW, the flow of surface waters in the west-
217 ern tropical Pacific is diverted more towards the North Pacific, feeding the
218 Kuroshio rather than the Indonesian Throughflow. This leads to a 50% de-
219 crease in the transport through the Indonesian Passages. A weakening of
220 the Aghulas Current, the North Brazil Current as well as the Gulf Stream
221 are also simulated (Figure 4). The formation of NPDW basically weakens
222 the whole surface branch of the global conveyor belt circulation (figure 4,
223 right panel). This relates also to a reduction of North Atlantic Deep Water
224 formation by 22% (from 27 to 21 Sv) (figure 3). In the Southern Ocean,
225 the zonally integrated overturning circulation in the bottom cell increases by
226 about 30% (from 17 to 22 Sv, not shown).

227 *3.2. Atmospheric response*

228 Due to the simulated North Pacific warming and reduced sea ice coverage,
229 the surface air temperature in the subpolar Pacific and over northern North
230 America increases by about 2°C (figure 6). This warming pattern causes a
231 reduction of the Subtropical High and an overall weakening of the tropical
232 trade winds. Anomalous advection of warm air over North America is likely
233 to contribute to the warming over Canada. We also observe a reduction
234 of the Westerlies in the Atlantic and an intensification of the Westerlies
235 over the Southern Ocean. The latter may be explained by an increased
236 meridional sea surface temperature (SST) gradient in this region (figure 2,
237 right panel), associated with a -5°C cooling equatorward of the southern

238 Ocean sea ice margin. The latter can be explained in terms of the heat
239 piracy argument (Seidov and Maslin, 2001). The meridional gradient of
240 equatorial Pacific SSTs and the resulting diabatic forcing (as characterized
241 by the precipitation anomalies in figure 6) leads to an intensification of the
242 southeasterly trade winds and a weakening of the northeasterly trades in the
243 Northern Hemisphere in agreement with simplified equatorial atmospheric
244 dynamics. The positive Wind-Evaporation SST feedback is likely to intensify
245 the trade wind anomalies in the eastern equatorial Pacific. The tropical SST
246 pattern is responsible for a northward shift of the Intertropical Convergence
247 Zone. Anomalous North Pacific precipitation patterns in the subtropics and
248 the extratropics can be directly linked to the weakened Subtropical High.

249 *3.3. Carbon cycle response*

250 Due to the stronger southeasterly trades and intensified southern hemi-
251 spheric Westerlies (figure 6), the upwelling in the Eastern Equatorial Pacific
252 and the Southern Ocean are enhanced, respectively. The globally reduced
253 stratification and associated enhanced mixing cause an enhanced transfer of
254 nutrients to the surface ocean. The globally averaged euphotic zone phos-
255 phate content thus increases by 25% with regional values in the eastern
256 equatorial and tropical Pacific attaining values of up to 60%. Changes in
257 the North Pacific and Southern Ocean are smaller and amount to 35% and
258 20%, respectively (figure 7, top panel).

259 As a result of the enhanced delivery of nutrients to the euphotic zone, the
260 export production increases globally by up to 20%. The strongest changes
261 are seen in the Eastern Equatorial and Tropical Pacific (+60%), the Eastern
262 Tropical Atlantic (+40%) and the North Pacific (+40%) (figure 7, middle

263 panel). As light is the main limiting factor of the marine production in the
264 polar Southern Ocean, despite the nutrient increase the export production
265 slightly decreases there due to sea ice advance.

266 Due to the enhanced mixing the euphotic silicate content also increases
267 by about 20%. This leads to 50% greater opal production in the North
268 Pacific and an increase of 20% in the Eastern Equatorial Pacific (figure 7,
269 bottom panel). In the Southern Ocean, the silicate content of the euphotic
270 zone increases by 45%. As the export production is actually reduced south
271 of Drake Passage, the anomalously high silicate concentrations are advected
272 to the southeastern Pacific and Atlantic. As a result, the opal production
273 intensifies by 30% in these regions .

274 There is a slight increase in CaCO_3 sedimentation rate (not shown) in
275 the Sea of Japan, the Kuril basin and off the west coast of North America
276 between the latitudes 35°N and 55°N . These changes are due to an enhanced
277 export production and increased CaCO_3 preservation.

278 The increased ventilation of deep water leads to greater dissolved oxygen
279 content in the deep part of the Atlantic and Pacific basins as well as in the
280 intermediate layers of the North Pacific and Southern Ocean (figure 8, top
281 panels). This version of the model calculates the ratio of ^{14}C over ^{12}C as a
282 tracer from which the ventilation age of the water masses is calculated. After
283 1,000 years of integration, the formation of NPDW leads to a substantial drop
284 in simulated ventilation ages in the North Pacific between 1,000 and 3,500 m
285 depth of about 1,000 years (figure 8, bottom left panel).

286 The increased mixing brings also more DIC to the surface (+4%). Even
287 though the enhanced export production leads to a greater flux of carbon from

288 the surface to the deep ocean, the surface DIC content still increases. This
289 leads to a greater CO₂ flux from the ocean to the atmosphere, namely in the
290 Eastern Equatorial Pacific (not shown). As a result of the competitive effects
291 of greater DIC transport to the surface and increased export production,
292 the oceanic carbon reservoir loses only about 18 GtC. On the other hand,
293 wetter conditions in the northern hemisphere induce a slightly greater carbon
294 storage on land (+8 GtC, not shown). The atmospheric CO₂ thus increases
295 by about 5 ppmv.

296 **4. Summary and Discussion**

297 Using an Earth system model of intermediate complexity we quantified
298 the effects of removing the subarctic North Pacific halocline on the large-scale
299 ocean circulation, global climate and the carbon cycle. It was demonstrated
300 that higher salinity in the North Pacific can trigger deep convection and
301 the formation of North Pacific Deep Water in the Bering Sea. Large-scale
302 adjustment processes in the ocean help to establish a Pacific Meridional Over-
303 turning Circulation which advects heat and salinity poleward. This PMOC
304 circulation does not exhibit any strong hysteresis behaviour, which is indica-
305 tive of a relatively weak Stommel feedback. The increased northward heat
306 transport initiates warming in the North Pacific and adjacent Canada as
307 well as a substantial cooling of the Southern Hemisphere. This behaviour
308 is consistent with the concept of the bipolar seesaw (Stocker, 1998). The
309 North Pacific warming induces a reduction of the subtropical high which
310 contributes to the warming of northern North America through anomalous
311 warm air advection. Otherwise the global wind changes are relatively small.

312 In our experiments global deep-water formation increases which requires
313 an intensification of diapycnal mixing of heat and tracers through a reduc-
314 tion in stratification. This response largely determines the biogeochemi-
315 cal changes simulated in our idealized sensitivity experiment. An enhanced
316 mixing of nutrients to the surface stimulates productivity and also export
317 production. In the Eastern Equatorial Pacific, export production is further
318 amplified by an intensification of southeasterly trade winds that lead to an
319 enhancement of upwelling. Changes of the surface DIC inventory partially
320 compensate the carbon sink due to increased export production and higher
321 terrestrial carbon uptake. It is concluded that the removal of the North
322 Pacific halocline has only a small bearing on atmospheric CO₂.

323 The presented results on the physical response are not entirely without
324 precedent. Using an OGCM coupled to an energy balance model (UVIC
325 model) as well as salinity compensation Saenko et al. (2004) also describe
326 the formation of a PMOC in result to higher North Pacific surface salini-
327 ties. In contrast to our results, Saenko et al. (2004) find a much stronger
328 response of the AMOC to the establishment of the PMOC. We repeated
329 experiment **FE** with salinity compensation (Stocker et al., 2007) but were
330 not able to reproduce the UVIC model results. In a North Pacific "de-
331 stratification" experiment performed with the Earth system of intermediate
332 complexity CLIMBER-2, a substantial warming of the North Pacific and of
333 Northern America is simulated, in accordance with our solution (Haug et al.,
334 2005). It is further argued that the sudden build-up of the NPH may have
335 helped to establish climate conditions that were more susceptible to ice-sheet
336 growth. Our simulated temperature response to a removal of North Pacific

337 surface stratification confirms their conjecture. Another important study
338 that elucidates the effects of higher North Pacific salinities during the early
339 and middle Pliocene is the modeling study by Motoi et al. (2005). Using an
340 older version of the GFDL Coupled General Circulation Model, the authors
341 find that opening Panama Isthmus leads to a weakening of the AMOC, in
342 agreement with Lunt et al. (2008) and Steph et al. (2010). The Panama
343 gateway opening allows a salinity transport from the Atlantic into the Pa-
344 cific which helps to establish a PMOC. Resulting changes in North Pacific
345 heat transport (~ 0.4 PW at 45°N) generate a widespread North Pacific and
346 North America warming that may have prevented the inception of glacial
347 cycles in response to orbital forcing changes in the early Pliocene.

348 Opal accumulation rates and nitrogen-isotope data from a marine sed-
349 iment core of the North Pacific (Haug et al., 1999) also suggest that the
350 establishment of the NPH in the mid-Pliocene had a significant impact on
351 the marine carbon cycle. Our model experiments presented here confirm the
352 notion of strongly enhanced North Pacific opal production and reduced nu-
353 trient utilization in the North Pacific in the absence of a NPH (Haug et al.,
354 1999), however they do not support the claim that the formation of a NPH
355 had a significant effect on atmospheric CO_2 .

356 Different processes can be responsible for causing high stratification in the
357 North Pacific. As suggested by Motoi et al. (2005) the closing of the Panama
358 Isthmus prevented high saline waters from the Caribbean from leaking into
359 the North Pacific. Moreover, it was demonstrated (Emile-Geay et al., 2003)
360 that under present-day conditions the atmospheric moisture transport across
361 Central America together with the east Asian monsoon play an important

362 role in maintaining the salinity gradient between Atlantic and Pacific. Both
363 of these atmospheric processes are strongly modulated through changes of
364 the AMOC (Okazaki et al., 2010; Kiefer, 2010). It should be noted here
365 that there exists quite some modeling uncertainty in regards to the question
366 whether a weakened AMOC leads to a reduced (Krebs and Timmermann,
367 2007; Leduc et al., 2007) or an intensified (Richter and Xie, 2010) moisture
368 transport across Central America. Paleo-data from different eras may provide
369 further insight into the direction of the moisture transport-AMOC feedback.

370 We realize that our study may well be relevant for the interpretation
371 of Pliocene climate-biogeochemical processes but its initial motivation was
372 to explain the global climate response to the potential onset of the PMOC
373 during Heinrich event 1. Evidence of increased ventilation of intermediate
374 to deep waters in the Northwest Pacific during Heinrich event 1 and the
375 YD was found in numerous marine sediment cores from the western North
376 Pacific (Ahagon et al., 2003; Ohkushi et al., 2004; Sagawa and Ikehara, 2008;
377 Okazaki et al., 2010), indicating the formation of NPDW during periods of
378 weak AMOC and the establishment of a Deep Western Boundary Current
379 in the North Pacific. Such conditions require a significant salinity increase
380 in the subarctic North Pacific which is in fact consistent with a salinity
381 reconstruction from marine sediment core GH02-1030 (Sagawa and Ikehara,
382 2008). The LOVECLIM model results presented in Okazaki et al. (2010)
383 further support the scenario of a disappearing halocline during Heinrich event
384 1 and probably even during the Younger Dryas.

385 From recent modeling studies (Zhang and Delworth, 2005; Timmermann
386 et al., 2007) it also becomes apparent that the climatic influence of an AMOC

387 shutdown on the Pacific, in absence of a PMOC, is opposite to the response
388 described here. Given that PMOC and AMOC are tightly coupled in a series
389 of model solutions (Mikolajewicz et al., 1997; Saenko et al., 2004; Krebs
390 and Timmermann, 2007; Okazaki et al., 2010) it can be concluded that the
391 detailed characteristics of millennial-scale North Pacific climate variations
392 during the Last Glacial Termination depend on a superposition of AMOC
393 and PMOC-related processes.

394 Reconstructing the detailed spatio-temporal behaviour of sea surface tem-
395 perature, salinity and ocean ventilation in the North Pacific during Glacial
396 Terminations will be an essential task that will further our understanding of
397 the operation of the Atlantic-Pacific seesaw and its role in shaping glacial
398 cycles.

399 **Acknowledgement**

400 This research was supported by NSF grant No. 1010869. Additional
401 support was provided by the Japan Agency for Marine-Earth Science and
402 Technology (JAMSTEC), by NASA through grant No. NNX07AG53G and
403 by NOAA through grant No. NA09OAR4320075, which sponsor research at
404 the International Pacific Research Center. A. Mouchet acknowledges support
405 from the Belgian Science Policy (BELSPO contract SD/CS/01A). *This is*
406 *IPRC publication number 724 and SOEST contribution number Y.*

407 **References**

408 Ahagon, N., Ohkushi, K., Uchida, M., Mishima, T., 2003. Mid-depth
409 circulation in the northwest Pacific during the last deglaciation: Ev-

410 idence from foraminiferal radiocarbon ages. *Geophys. Res. Lett.* 30,
411 doi:10.1029/2003GL018287.

412 Brovkin, V., Ganopolski, A., Svirezhev, Y., 1997. A continuous climate-
413 vegetation classification for use in climate-biosphere studies. *Ecol. Modell*
414 101, 251–261.

415 Campin, J., Goosse, H., 1999. Parameterization of density-driven downslop-
416 ing flow for a coarse-resolution ocean model in z-coordinate. *Tellus* 51A,
417 412–430.

418 Emile-Geay, J., Cane, M., Naik, N., Seager, R., Clement, A., van
419 Geen, A., 2003. Warren revisited: Atmospheric fluxes and "Why is
420 no deep water formed in the North Pacific". *J. Geophys. Res.* 108,
421 doi:10.1029/2001JC001058.

422 Fichefet, T., Driesschaert, E., Goosse, H., Huybrechts, P., Janssens,
423 I., Mouchet, A., Munhoven, G., 2007. Modelling the evolution of
424 climate and sea level during the third millennium (MILMO)*http* :
425 *//www.belspo.be/belspo/home/publ/pub_ostc/EV/rappEV09_en.pdf*.

426 Goosse, H., Brovkin, V., Fichefet, T., Jongma, J., Huybrechts, P., Mouchet,
427 A., Barriat, P.-Y., Campin, J.-M., Deleersnijder, E., Driesschaert, E.,
428 Goelzer, H., Haarsma, R., Janssens, Y., Loutre, M.-F., Maqueda, M.
429 A. M., Opsteegh, T., Mathieu, P.-P., Munhoven, G., Petterson, E.,
430 Renssen, H., Roche, D., Schaeffer, M., Selten, F., Severijns, C., Tartinville,
431 B., Weber, N., 2010. Description of the Earth system model of intermedi-

- 432 ate complexity LOVECLIM version 1.2. Geoscientific Model Development,
433 submitted.
- 434 Goosse, H., Deleersnijder, E., Fichefet, T., England, M., 1999. Sensitivity of
435 a global coupled ocean-sea ice model to the parameterization of vertical
436 mixing. *J. Geophys. Res.* 104(C6), 13681–13695.
- 437 Goosse, H., Fichefet, T., 1999. Importance of ice-ocean interactions for the
438 global ocean circulation: a model study. *J. Geophys. Res.* 104(C10), 23337–
439 23355.
- 440 Haug, G., Ganopolski, A., Sigman, D., Rosell-Mele, A., Swann, G., Tiede-
441 mann, R., Jaccard, S., Bollmann, J., Maslin, M., Leng, M., Eglinton, G.,
442 2005. North Pacific seasonality and the glaciation of North America 2.7
443 million years ago. *Nature* 433, 821–825.
- 444 Haug, G., Sigman, D., Tiedemann, R., Pedersen, T., Sarnthein, M., 1999.
445 Onset of permanent stratification in the subarctic Pacific Ocean. *Nature*
446 401, 779–782.
- 447 Hu, A., Meehl, G., 2005. Bering Strait throughflow and the thermohaline
448 circulation. *Geophys. Res. Lett.* 32, doi:10.1029/2005GL024424.
- 449 Kiefer, T., 2010. When Still Waters Ran Deep. *Science* 329, 290–291.
- 450 Krebs, U., Timmermann, A., 2007. Tropical air-sea interactions accelerate
451 the recovery of the Atlantic Meridional Overturning Circulation after a
452 major shutdown. *J. Climate* 20, 4940–4956.

- 453 Leduc, G., Vidal, L., Tachikawa, K., Rostek, F., Sonzogni, C., Beaufort, L.,
454 Bard, E., 2007. Moisture transport across Central America as a positive
455 feedback on abrupt climatic changes. *Nature* 445, 908–911.
- 456 Lim, G., Holton, J., Wallace, J., 1991. The structure of the ageostrophic
457 wind field in baroclinic waves. *J. Atmos. Sci.* 48, 1733–1745.
- 458 Lunt, D. J., Valdes, P. J., Haywood, A., Rutt, I., 2008. Closure of the Panama
459 Seaway during the Pliocene: implications for climate and Northern Hemi-
460 sphere glaciation. *Clim. Dyn.* 30, 1–18.
- 461 McManus, J. F., Francois, R., Gherardi, J. M., Keigwin, L. D., Brown-Leger,
462 S., 2004. Collapse and rapid resumption of Atlantic meridional circulation
463 linked to deglacial climate changes. *Nature* 428, 834–837.
- 464 Menviel, L., Timmermann, A., Mouchet, A., Timm, O., 2008. Meridional re-
465 organizations of marine and terrestrial productivity during Heinrich events.
466 *Paleoceanography* 23, doi:10.1029/2007PA001445.
- 467 Mikolajewicz, U., Crowley, J., Schiller, J., Voss, R., 1997. Modeling telecon-
468 nections between the North Atlantic and North Pacific during the Younger
469 Dryas. *Nature* 387, 384–387.
- 470 Motoi, T., Chan, W.-L., Minobe, S., Sumata, H., 2005. North Pa-
471 cific halocline and cold climate induced by Panamanian Gateway clo-
472 sure in a coupled ocean-atmosphere GCM. *Geophys. Res. Lett.* 32,
473 doi:10.1029/2005GL022844.
- 474 Mouchet, A., Francois, L., 1996. Sensitivity of a Global Oceanic Carbon Cycle

- 475 Model to the circulation and to the fate of organic matter: preliminary
476 results. *Physics and Chemistry of Earth* 21, 511–516.
- 477 Ohkushi, K., Uchida, M., Ahagon, N., Mishima, T., Kanematsu, T., 2004.
478 Glacial intermediate water ventilation in the northwestern Pacific based
479 on AMS radiocarbon dating. *Nucl. Instr. and Meth. B* 223-224, 460–465.
- 480 Okazaki, Y., Timmermann, A., Menviel, L., Harada, N., Abe-Ouchi, A.,
481 Chikamoto, M., Mouchet, A., Asahi, H., 2010. Deep water formation in
482 the North Pacific during the Last Glacial termination. *Science* 329, 200–
483 204.
- 484 Opsteegh, J., Haarsma, R., Selten, F., Kattenberg, A., 1998. ECBILT: A
485 dynamic alternative to mixed boundary conditions in ocean models. *Tellus*
486 50A, 348–367.
- 487 Richter, I., Xie, S.-P., 2010. Moisture transport from the Atlantic to the Pa-
488 cific basin and its response to North Atlantic cooling and global warming.
489 *Clim. Dyn.* 35, 551–566.
- 490 Saenko, O., Schmittner, A., Weaver, A., 2004. The Atlantic-Pacific seesaw.
491 *J. Climate* 17, 2033–2038.
- 492 Sagawa, T., Ikehara, K., 2008. Intermediate water ventilation change in the
493 subarctic northwest Pacific during the last deglaciation. *Geophys. Res.*
494 *Lett.* 35, doi:10.1029/2008GL035133.
- 495 Seidov, D., Maslin, M., 2001. Atlantic Ocean heat piracy and the bipolar
496 climate see-saw during Heinrich and Dansgaard-Oeschger events. *J. Quat.*
497 *Sci.* 16, 321–328.

- 498 Steph, S., Tiedemann, R., Prange, M., Groeneveld, J., Schulz, M., Timmer-
499 mann, A., Nürnberg, D., Rühlemann, C., Saukel, C., Haug, G., 2010. Early
500 Pliocene increase in thermohaline overturning: A precondition for the de-
501 velopment of the modern equatorial Pacific cold tongue. *Paleoceanography*
502 25, doi:10.1029/2008PA001645.
- 503 Stocker, T., 1998. The seesaw effect. *Science* 282, 61–62.
- 504 Stocker, T., Timmermann, A., Renold, M., Timm, O., 2007. Effects of
505 salt compensation on the climate model response in simulations of large
506 changes of the Atlantic Meridional Overturning Circulation. *J. Climate* 20,
507 5912–5928.
- 508 Timmermann, A., Lorenz, S., An, S. I., Clement, A., Xie, S.-P., 2007. The Ef-
509 fect of Orbital Forcing on the Mean Climate and Variability of the Tropical
510 Pacific. *J. Clim.*, 41474159.
- 511 Warren, B., 1983. Why is no deep water formed in the North Pacific? *J.*
512 *Mar. Res.* 41, 327–347.
- 513 Zhang, R., Delworth, T., 2005. Simulated tropical response to a substantial
514 weakening of the Atlantic thermohaline circulation. *J. Climate* 18, 1853–
515 1860.

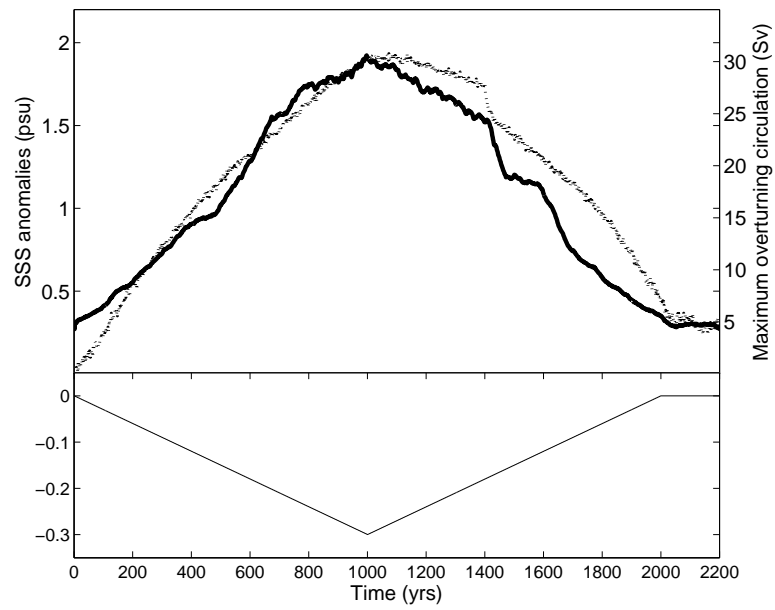


Figure 1: (top) Sea surface salinity anomalies averaged over the area 150-230°E, 50-60°N (dashed line) and maximum overturning strength (Sv) in the North Pacific (solid line) for FE compared to PIN. (bottom) Anomalous negative freshwater input in the area 150-230°, 47-63°N.

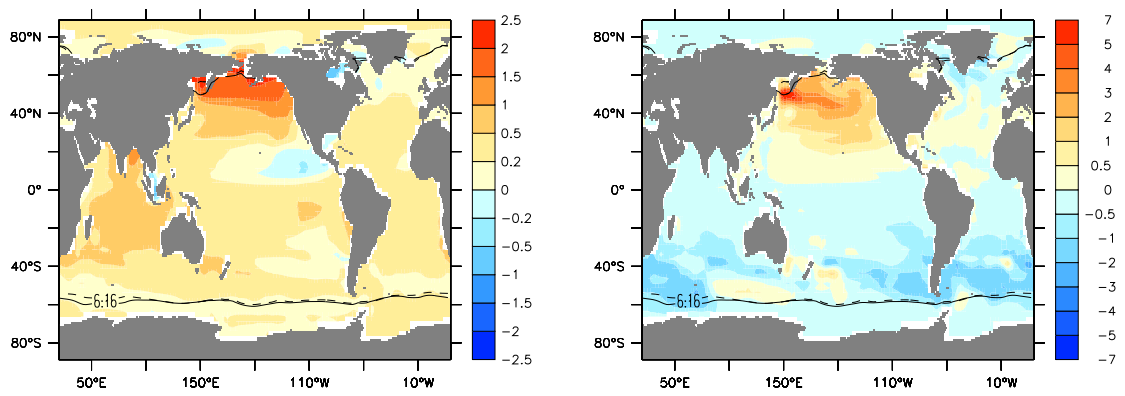


Figure 2: (left) Sea surface salinity anomalies. (right) Sea surface temperature anomalies ($^{\circ}\text{C}$). The contour lines represent the 0.1 m sea ice level for PIN (solid line) and FE averaged over years 900–1000 (dashed line). Anomalies are for FE averaged over years 900–1000 compared to PIN.

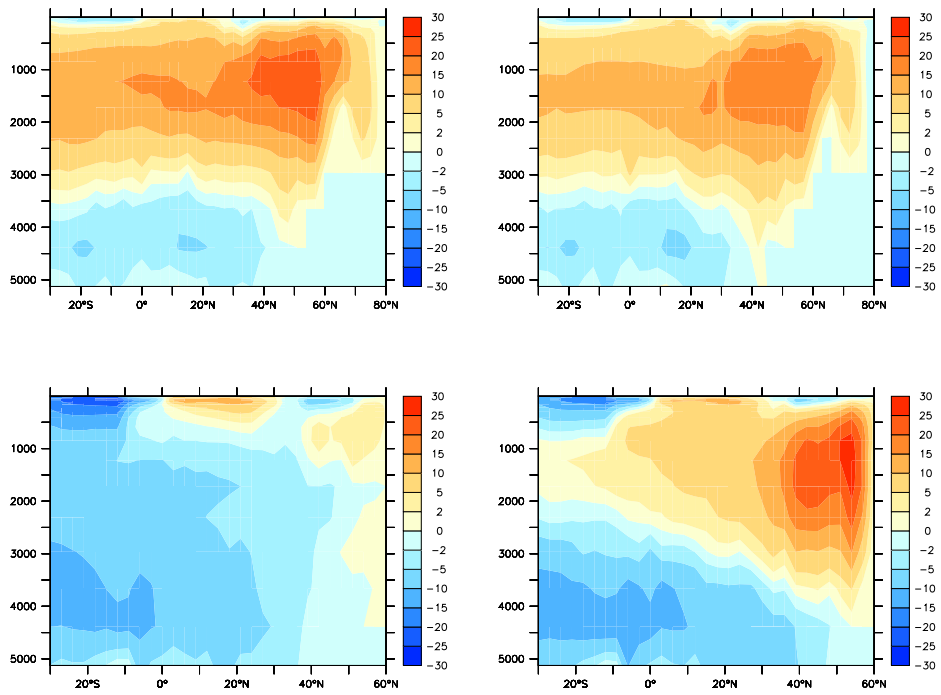


Figure 3: Stream function averaged over the Atlantic basin for (top left) PIN and (top right) FE at years 900–1000. Stream function averaged over the Pacific basin for (bottom left) PIN and (bottom right) FE at years 900–1000.

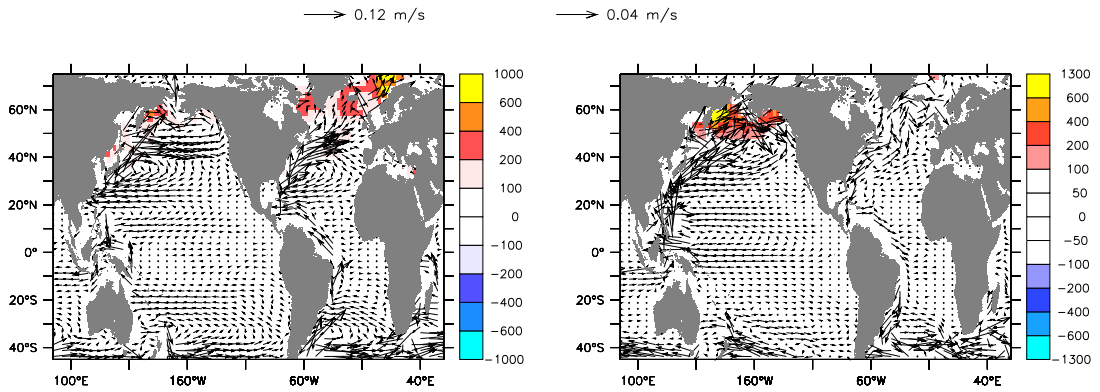


Figure 4: (left) Winter (DJF) mixed layer depth averaged for PIN (shaded) and currents (m/s) averaged over the depths 0–500 m for PIN. (right) Winter (DJF) mixed layer depth anomalies averaged over years 900–1000 for FE compared to PIN (shaded). Current anomalies (m/s) averaged over the depths 0–500 m and over years 900–1000 for FE compared to PIN.

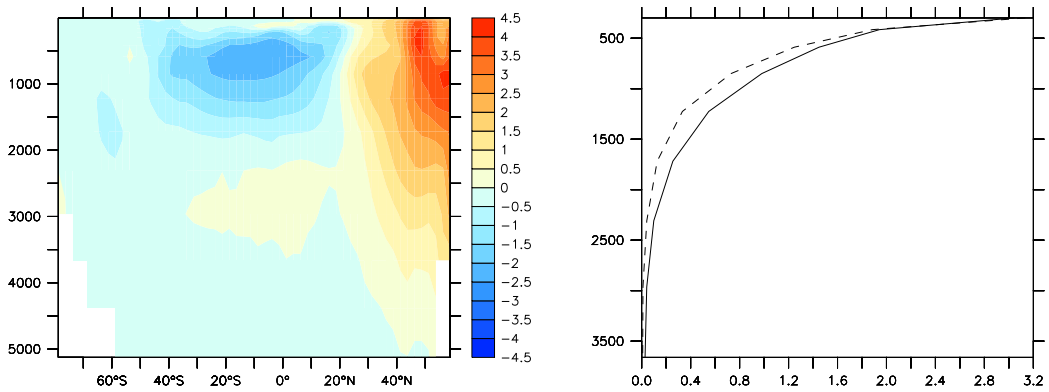


Figure 5: (left) Temperature anomaly ($^{\circ}\text{C}$) averaged over the Pacific basin for FE averaged over years 900–1000 compared to PIN. (right) Density gradient (g/m^4) averaged over the Pacific basin for PIN (solid line) and for FE averaged over years 900–1000 (dashed line)

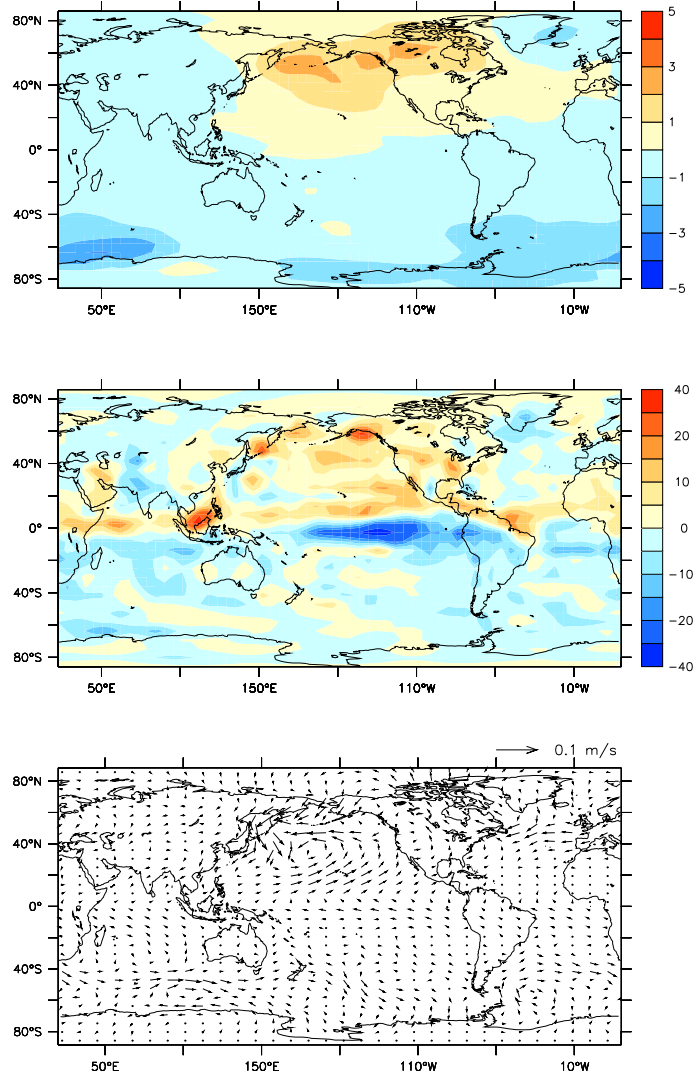


Figure 6: (top) Air temperature anomalies ($^{\circ}\text{C}$), (middle) precipitation anomalies (cm/yr) and (bottom) windstress anomalies (Pa). Anomalies are for FE averaged over years 900–1000 compared to PIN.

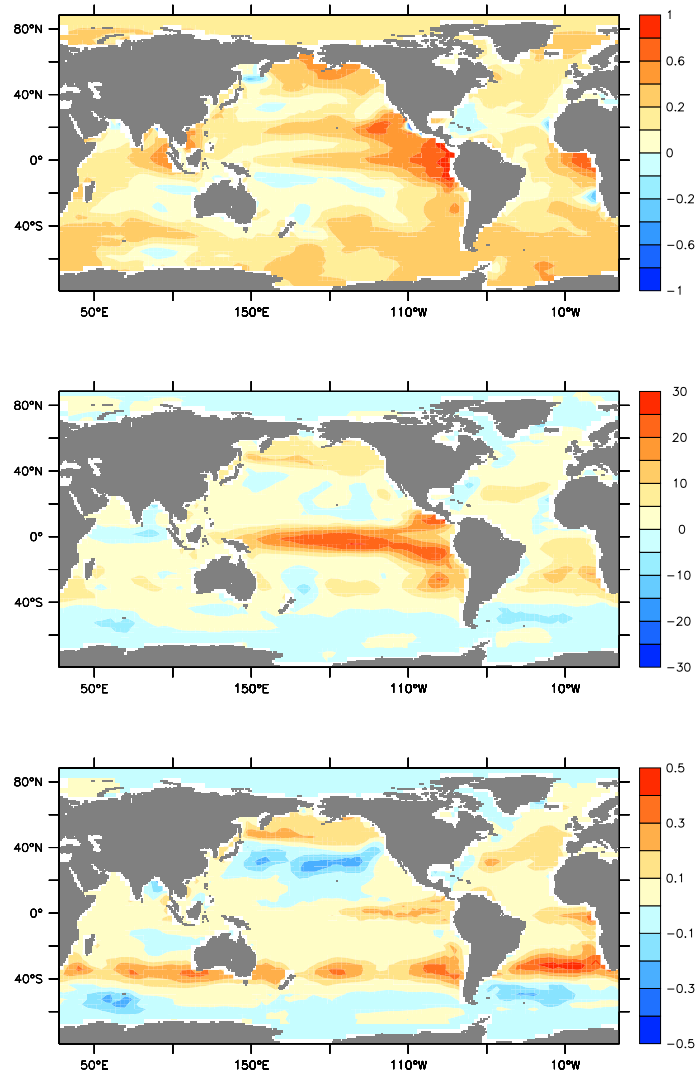


Figure 7: (top) Phosphate anomalies ($\mu\text{mol/l}$) averaged over the euphotic zone, (middle) export production anomalies ($\text{gC/m}^2/\text{yr}$) and (bottom) opal production anomalies ($\text{mol/m}^2/\text{yr}$). Anomalies are for FE at year 1000 compared to PIN.

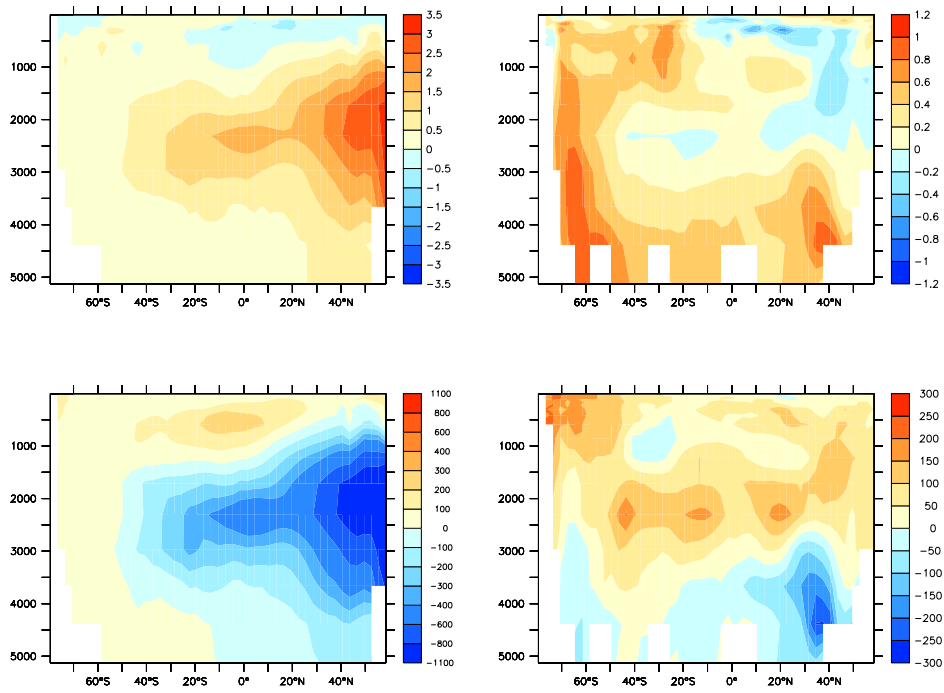


Figure 8: (top left) Oxygen anomalies (ml/l) in the Pacific basin and (top right) in the Atlantic basin at year 1000 compared to PIN. Ventilation age anomalies (in years) for (bottom left) the Pacific basin and (bottom right) the Atlantic basin at year 1000 compared to PIN.